

Lasers in Manufacturing Conference 2023

Defects formation in ultrafast laser machined glass

Jan Novotný^{a,*}, Libor Mrňa^a

^a*Institute of Scientific Instruments of the CAS, v. v. i., Královopolská 147, Brno, 61200, Czech Republic*

Abstract

Ultrafast lasers are a versatile tool for processing all materials, but especially very hard and brittle ones due to the non-contact nature of the process. Forming free-form structures, such as those needed for micro-optics or microfluidics is still a challenging task, where ultrafast lasers can be exploited conveniently. Although only minimal heat and mechanical stress are exerted during processing, defects that hinder intended use can still develop. Limiting these defects through using the right settings leads to faster and simpler finishing of fabricated parts. We present the results of using $\approx 1\text{ps}$ 1030nm laser to produce structures in fused silica. Formation of cracks, recast material, and excessive roughness is studied to set appropriate parameters of the ablation process.

Keywords: Ultrafast laser; laser ablation; glass, defects

1. Introduction

Ultrafast lasers can be a versatile tool for the production of free-shape, multi, or micro-optics that are difficult or even impossible to create by traditional methods. Yang et al., 2022 reported a varying numerical aperture microlens array manufacturing by wet etching of an initial femtosecond laser ablated channels in a K9 glass substrate. Schwarz et al., 2021, produced a top-hat beam homogenizer using an all-laser process consisting of ultrafast laser ablation of the designed shape followed by CO₂ laser polishing resulting in a good-quality optical element. Dudutis et al., 2020, compared an axicon produced by the same sequence as Schwarz et al. with commercially available axicons. They showed a competitive quality with standard-quality mass-produced elements.

Although laser ablation does not yield surfaces of optical quality, the non-contact nature of the process can be beneficial if elements are finished properly. The absence of impurities and damage precursors that originate

* Corresponding author. Tel.: +420 541 514 338.
E-mail address: jann@isibrno.cz.

from contact manufacturing processes is reported to increase LIDT values by more than 30 % (Cao et al., 2020). A suitable processing strategy must be chosen to obtain a good preform of an optical element without defects, such as cracks or recast material, or excessive roughness/waviness. Although ultrafast lasers ablate material in an athermal way, mechanical and structural damage to the material is caused by local heating (and induced stresses of the material from the heat accumulation effect). The impact of several process parameters - laser fluence (pulse energy), scanning speed and pulse overlap, change of scanning trajectory angle, and interlacing was tested in this paper to obtain the best roughness of the ablated surface and assess conditions when other defects occur. Then the samples were etched to reveal subsurface defects.

2. Experimental

Polished fused silica samples of thickness 2 mm were processed using PERLA 100 (HiLASE Centre) ultrafast thin-disc laser system combined with intelliSCAN_{se} 14 (SCANLAB) galvanometric scan head. A linearly polarized gaussian output beam of diameter approx. 3 mm and M^2 1.3 was expanded to 9 mm diameter and focused onto the top surface of the samples using 100 mm focal length telecentric F-theta lens (LINOS) resulting in a focal spot diameter (w_f) of about 25 μm . The experiment was carried out using a fundamental wavelength of 1030 nm (2nd and 4th harmonics possible), pulse width < 2 ps, and repetition frequency 60 kHz. Maximum laser pulse energy 1 mJ was modulated using a polarizing attenuator to obtain desired energy behind the focusing lens. The resulting average power was measured at the output of the focusing lens by S415C thermal power meter (Thorlabs) and pulse energy was calculated using a fixed repetition frequency.

On each fused silica specimen, an array (Fig. 1) of rectangular cavities of dimensions 2.8 mm \times 2.8 mm was machined using different scanning parameters and fluence. Höhm et al., 2012 and Nieto et al., 2015, reported threshold fluence of fused silica as $F_{th} = 3.45 \text{ J}\cdot\text{cm}^{-2}$ and $3.6 \text{ J}\cdot\text{cm}^{-2}$, respectively (for slightly shorter wavelengths and pulse lengths). Therefore, a value $F_{th} = 4 \text{ J}\cdot\text{cm}^{-2}$ was considered for the design of the experiment. Areas were scanned by lines of alternating directions with line spacing L_s and a constant scan velocity v_s , resulting in pulse separation s_s .

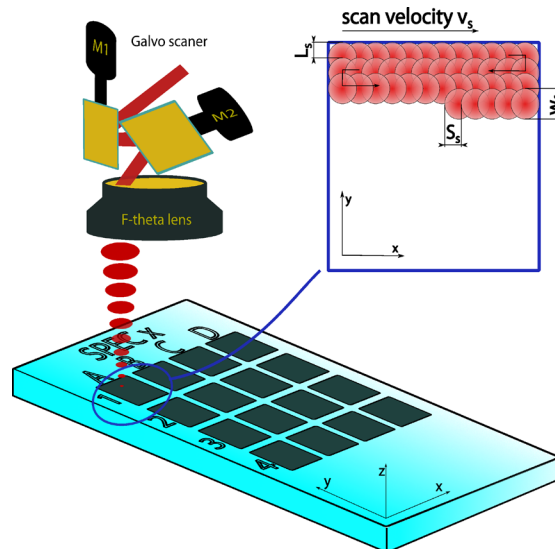


Fig. 1. Schematic of specimen processing

For evaluating the effects of laser fluence, scan speed, and line (hatching) spacing – heat accumulation effects - two samples (spec1 and 2) were processed using parameters according to Table. 1. Peak laser fluence F_{peak} was set to be 1, 1.5, 3 and 6 times F_{th} ($w_f = 25 \mu\text{m}$) and corresponding laser energy was calculated according to Eq. 1. Scan speed and line overlap were set so the resulting spots per area (SPA) number – SPA_s in the scan direction Eq. 2 and SPA_l in the hatching direction - Eq. 3, is equal to 2, 5 and 10. Areas were scanned repeatedly so the resulting number of pulses on each area is the same.

$$E_p = F_{peak} * \frac{\pi}{2} * \left(\frac{w_f}{2}\right)^2 \quad (1)$$

$$SPA_s = \frac{w_f * f_{rep}}{v_s} \quad (2)$$

$$SPA_l = \frac{w_f}{L_s} \quad (3)$$

Table 1. Laser and scan parameters were used for processing specimens 1 and 2.

| F_{peak} [$\text{J}\cdot\text{cm}^{-2}$] | E_p [nJ] | P_{av} [mW] | SPA | v_s [$\text{mm}\cdot\text{s}^{-1}$] | L_s [mm] |
|--|------------|---------------|-----|---|------------|
| 4 | 9.8 | 589 | 2 | 750 | 0.0125 |
| 6 | 14.7 | 884 | 5 | 300 | 0.005 |
| 12 | 29.5 | 1777 | 10 | 150 | 0.0025 |
| 24 | 58.9 | 3530 | | | |

Effects of line interlacing and hatching angle change were tested on specimen 3. The basic pattern of linear hatching (spacing $2.5 \mu\text{m}$) was altered by interlacing with coefficients 1, 2, 5 and 10 (every n-th line is scanned in one pass in n-passes). All areas were processed using fluence $12 \text{ J}\cdot\text{cm}^{-2}$ and a constant scan speed $600 \text{ mm}\cdot\text{s}^{-1}$. Angles were changed by increments of 180° , 90° , 45° and 16.6° . Each area was scanned 10 times (about 55 s per area). After processing, samples were cleaned in an ultrasonic cleaner for 5 minutes in demineralized water and then analysed using a confocal laser scanning microscope (Keyence VK-X) and contact profile measurement device Talystep (Taylor Hobson).

Spec 1 was then wet etched to remove partially crystallised material and recast. Spec 1 was etched for 80 minutes in total in an oxide-buffered solution of hydrofluoric acid (BOE 7:1 VLSI (Microchemicals)) with mechanical agitation (250 RPM). Based on previous experience and datasheet, the expected etched depth in undamaged fused silica was $7 - 8 \mu\text{m}$ ($80 - 100 \text{ nm}\cdot\text{min}^{-1}$). Then, the etched depth and resulting surface were measured using the laser microscope.

3. Results

3.1. Heat accumulation (Spec 1 and 2)

Table 2 shows resulting area (S_a) and profile (R_a) average roughness of the spec 1 and 2 after the laser processing and depth of the cavity combined with defect indication. Only completely ablated samples were measured. The green underlying colour indicates an uneven and rough surface (an example of such surface

can be found in Fig 2 – D2 area). The red colour of values is used for indication of edge chipping. The orange colour of the cell show occurrence of areas ablated to a greater depth than surrounding areas (craters). Blue text colour is used for indication of highly periodic surface formation with period equal to L_s - 12.5 μm .

Table 2. Resulting surface (S_a , S_{filter} 0.05 mm) profile (R_a , λ_c 0.25 mm) roughness, depth and defect occurrences on Spec 1 and 2. The difference in S_a and R_a values originates in different low-pass filter (S_{filter} , λ_c) settings, where larger structures are included in profile roughness measurement only.

| Spec | Row | v_s [mm.s ⁻¹] | S_a [μm] / R_a [μm] | | Column | | | |
|------|-----|--------------------------------|---|----------------|------------------------------------|-----------------------|---------------------|----------------------|
| | | | L_s [mm] | Repeats [-] | Peak fluence [J.cm ⁻²] | | | |
| | | | | | A 4 | B 6 | C 12 | D 24 |
| 1 | 1 | 150 | 0.0025 | 1 | N/A (19.9) | 0.334/0.346 33 | 0.344/0.745 58 | 0.679/0.986 90.1 |
| | 2 | 300 | 0.005 | 4 | N/A 0 | 0.391/0.482 44 | 0.322/0.395 70.3 | 0.602/1.637 139.5 |
| | 3 | 750 | 0.0125 | 25 | N/A 0 | 0.515/0.553 26.7 | 0.411/0.421 56.9 | 0.395/0.370 97.3 |
| 2 | 1 | 750 | 0.0025 | 5 | N/A 0 | 0.400/0.422 46.1 | 0.371/0.368 69.9 | 0.551/1.161 148.3 |
| | 2 | 300 | 0.005 | 4 | N/A 0 | 0.396/0.463 44.3 | 0.364/0.344 72.6 | 0.619/2.217 142.2 |
| | 3 | 150 | 0.0125 | 5 | N/A 0 | 0.530/0.837 40.568 | 0.449/0.472 75.5 | 0.425/0.481 129 |

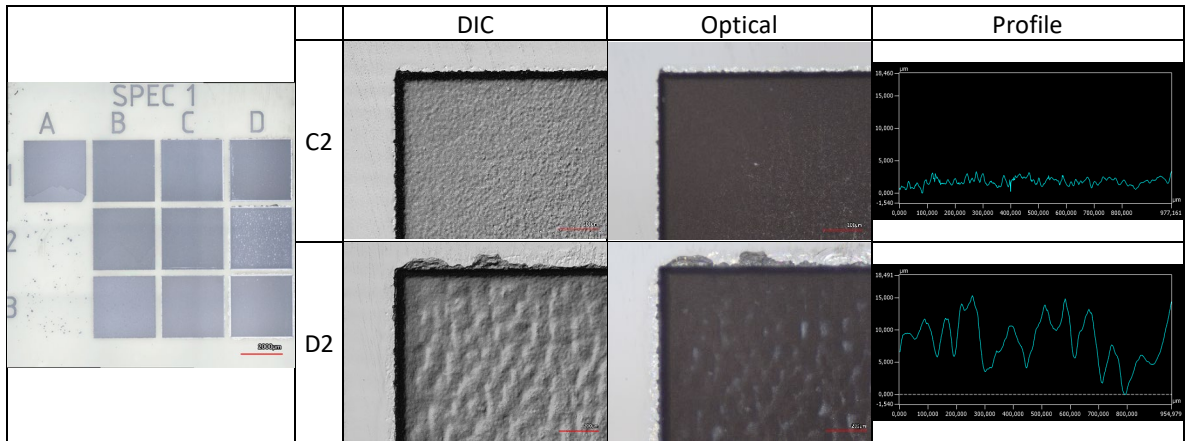


Fig. 2. Comparison of areas C2 and D2 on Spec 1, D2 shows typical defects – edge chipping, uneven surface, and traces of recast material (white areas on optical image). Profiles have same Z-axis size, scale 200 μm .

Some recast material, that was not removed by cleaning was observed on the edges of the “D” samples. Most of the defects were observed within areas where the lowest line spacing was used, especially combined with higher pulse energy and low scan speed. Areas with high spots-per-area number yielded the worst surface

roughness and overall quality. The best results were observed when moderate scanning parameters were used (C2 areas) with the resulting surface roughness of around $0.35 \mu\text{m}$ and material removal of around $0.75 \text{ mm}^3 \cdot \text{min}^{-1}$. The highest material removal was observed in areas D1 and D2 on Spec 2 and D2 on Spec 1, where severe edge chipping was also observed indicating, that the material is removed in larger chips due to thermal stress cracking. Areas D3 on both specimens were correctly processed (material removal more than $1.1 \text{ mm}^3 \cdot \text{min}^{-1}$) indicating rather secondary importance of scan speed for resulting quality. The periodic surface of the samples B3 and C3 is the most probably not observed because of beam size change based on the F_{peak} value.

Within Spec 1/A1 area, as on the only one processed with $F_{peak} = 4 \text{ J} \cdot \text{cm}^{-2}$, nearly complete ablation was achieved, probably due to high spots-per-area number in both directions. On other areas in column A only a localized ablation was achieved, probably as a result of impurities in/on the substrate. In closer examination of area Spec 1/A3, a distinguishable dot matrix of slightly ablated structures (diameter $6 \mu\text{m}$, spacing $12.5 \mu\text{m}$) was observed.

3.2. Hatching angle change (Spec 3)

Table 3 shows the results of roughness and depth measurement on Spec 3. Although the areas processed with low interlacing (column A) showed a similar roughness as those processed with the higher interlacing, severe creation of local craters of depth up to $10 \mu\text{m}$ was observed. Edge chipping also occurred on samples within this column. This is demonstrated in Fig. 3, where the resulting surfaces of areas from row 3 are shown. Ablated depths of areas without visible defects were measured to be very similar to each other (see Columns B, C in Table. 3). High-interlaced column D showed a slightly higher ablation depth in contrast to more closely hatched areas, but at the cost of high-roughness.

Table 3. Resulting surface (S_a , S_{filter} 0.05 mm) and profile roughness (R_a , λ_c 0.25 mm), depth and defect occurrences on Spec 3, orange colour of the cell used for areas with local craters, blue for a visible periodic structure.

| Row | S_a [μm] / R_a [μm] Depth [μm] | Scan speed $v_s = 600 \text{ mm} \cdot \text{s}^{-1}$ ($SPA_s = 2.5$) | | | | | | | |
|-----|--|---|----------------------|---|----------------------|---|---------------------|---|---------------------|
| | | Column – Interlacing (Effective spacing) [mm] | | | | | | | |
| | Angle increment | A | 1 (0.0025) | B | 2 (0.005) | C | 5 (0.0125) | D | 10 (0.025) |
| 1 | 180 ° | | 0.371/0.464 99.6 | | 0.363/0.462 107.1 | | 0.385/0.369 91.8 | | 0.618/0.523 98.0 |
| 2 | 90 ° | | 0.311/0.422 99.8 | | 0.353/0.359 90.0 | | 0.371/0.364 91.1 | | 0.599/0.552 95.9 |
| 3 | 45 ° | | 0.297/0.469 99.4 | | 0.337/0.332 91.0 | | 0.381/0.380 91.8 | | 0.629/0.541 97.8 |
| 4 | 16.6 ° (10 directions) | | 0.356/0.478 100.5 | | 0.356/0.316 91.8 | | 0.379/0.352 92.2 | | 0.530/0.549 98.9 |

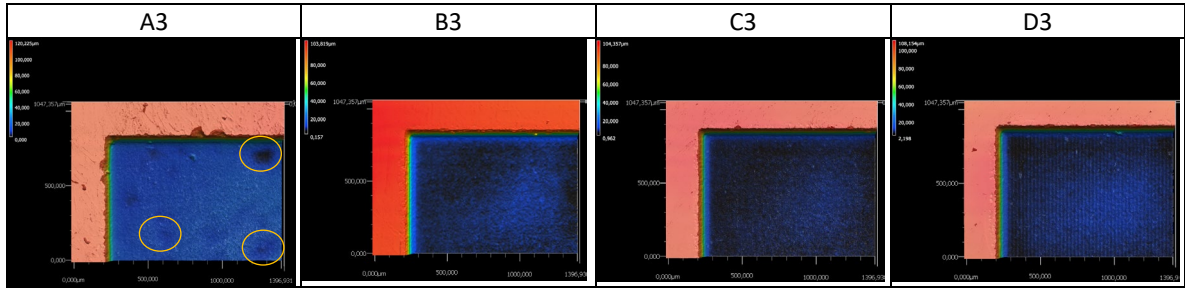


Fig. 3. Height images of areas on Spec 3, yellow ellipses on A3 show locations of craters. Visible linear periodic structures on D3 (note that “higher” – lighter blue areas on images are microscope related, as they are observed on most of the images).

3.3. Etching

The etching of the sample caused creation of a mostly chaotic structure. Samples in columns B and C showed similar behaviour – random, bubble-like structures (example on Fig. 4 – Spec 1 C2) with S_a exceeding $2 \mu\text{m}$ and S_z (maximal height) $15 \mu\text{m}$. In area B3, a highly regular periodic structure composed of circular holes of depth at least $10 \mu\text{m}$ (missing microscope data in central – deep – part), diameter $11 \mu\text{m}$ and spacing of $25 \mu\text{m}$ (double of the original periodicity of the sample surface). In column D surface is formed of the random channels of width and depth both approx. $13 \mu\text{m}$, which might originate in sub-surface cracks.

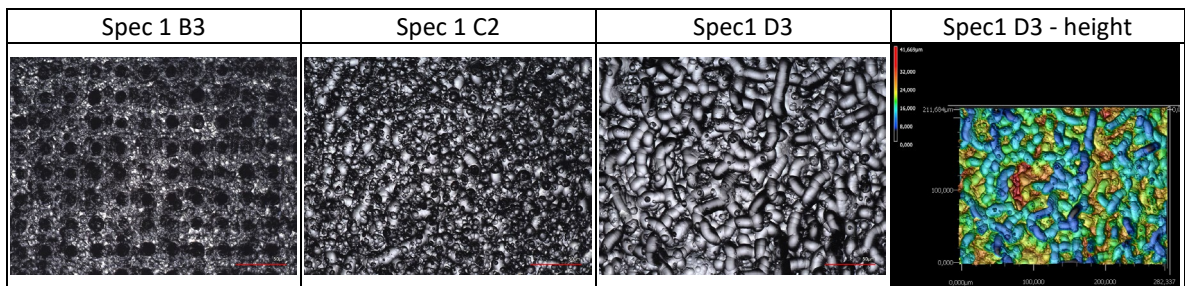


Fig. 4. Structures formed after etching on Spec 1 (scale $50 \mu\text{m}$).

Samples in column B were etched to a depth of around $22 \mu\text{m}$, in column C to $24 \mu\text{m}$. Samples D2 and D3 were etched to a depth of $42 \mu\text{m}$ and $40 \mu\text{m}$ respectively. Although all areas were etched in the same process, the D1 area was measured to be $13 \mu\text{m}$ on average deeper than before etching. The original polished surfaces of the glass sample showed damage after etching – random dimples approx. $4 \mu\text{m}$ in diameter.

4. Conclusions and discussion

The influence of several process parameters on resulting surface quality and material damage was tested. As only partial ablation was observed for the lowest fluence setting, (nearly) a single pulse threshold fluence for laser used in this study is slightly higher than $4 \text{ J}\cdot\text{cm}^{-2}$. The observed dot-matrix on Spec 1/A3, where 25 pulses were cumulatively incident in a one spot indicates, that threshold fluence was lowered enough to enable modification of the fused silica. For the highest fluence settings, a very rough surface and chipped edges were typically observed, so a suitable fluence processing window falls between $6 \text{ J}\cdot\text{cm}^{-2}$ and at least $12 \text{ J}\cdot\text{cm}^{-2}$. When the most favourable parameters are set, a processing with a fluence of $24 \text{ J}\cdot\text{cm}^{-2}$ is possible with material

removal higher than $1.1 \text{ mm}^3 \cdot \text{s}^{-1}$, but with possible sub-surface damage as a higher etch rate is usually associated with the material damage.

Hatching line spacing was observed as a very important parameter which should be carefully set. The low L_s causes a very-likely random chipping of the glass, which results in craters and relates to the edge chipping. The high L_s results in a periodic structure on the processed material, which increases its roughness/waviness. Scan speed has a lower effect on results than hatch spacing, which can be caused by a nearly immediate (on thermal-time scales) incidence of subsequent pulse, when even the lowest speed does not allow for a significant temperature rise in this direction. While an effective speed in the L_s direction (perpendicular to v_s) is much lower, so heat can travel further between each line.

Angle change did not have any effect on the resulting quality and ablation efficiency. Interlacing has a similar effect to line spacing. When an effective line spacing was set to be equal to a spot size, an increase in ablation depth was observed. This change also resulted in increased roughness and visible periodic structure of the surface. The traces of only the last scan direction were observed.

Etching removed a significantly higher amount of the material than expected, which was caused by sub-surface laser modification resulting in a higher etching rate. The resulting surface roughness was an order of magnitude higher than laser-processed samples. At lower fluences, a bubble-like structure formed, which might originate in point defects in the Z direction. At high fluence, random channel structure evolved that might be caused by etching of vertical planar defects – cracks. For the next research, a more suitable etching method and parameters should be chosen. We plan to repeat experiments using a reactive-ion etching and CO₂ laser polishing. It would be beneficial in the next experiments to calculate SPA based on a spot size defined by the threshold fluence of a material used in the experiment in combination with a particular F_{peak} value to provide more consistent results.

Acknowledgements

This contribution was created within the framework of project TN02000020 entitled Center of Advanced Electron and Photon Optics and is co-financed with the state support of the Technology Agency of the Czech Republic within the Program for the Support of Applied Research, Experimental Development and Innovation of the National Center of Competence".

References

- Cao, Zhen, Chaoyang Wei, Xin Cheng, Yuanan Zhao, Xiacong Peng, Zhigang Jiang, a Jianda Shao. 2020. „Ground Fused Silica Processed by Combined Chemical Etching and CO₂ Laser Polishing with Super-Smooth Surface and High Damage Resistance". *Optics Letters* 45 (21): 6014–17. <https://doi.org/10.1364/OL.409857>.
- Dudutis, Juozas, Jokūbas Pipiras, Simon Schwarz, Stefan Rung, Ralf Hellmann, Gediminas Račiukaitis, a Paulius Gečys. 2020. „Laser-Fabricated Axicons Challenging the Conventional Optics in Glass Processing Applications". *Optics Express* 28 (4): 5715–30. <https://doi.org/10.1364/OE.377108>.
- Höhm, S., A. Rosenfeld, J. Krüger, a J. Bonse. 2012. „Femtosecond Laser-Induced Periodic Surface Structures on Silica". *Journal of Applied Physics* 112 (1): 014901. <https://doi.org/10.1063/1.4730902>.
- Nieto, Daniel, Justo Arines, Gerard M. O'Connor, a María Teresa Flores-Arias. 2015. „Single-Pulse Laser Ablation Threshold of Borosilicate, Fused Silica, Sapphire, and Soda-Lime Glass for Pulse Widths of 500 Fs, 10 Ps, 20 Ns". *Applied Optics* 54 (29): 8596. <https://doi.org/10.1364/AO.54.008596>.
- Schwarz, Simon, Babette Götzendorfer, Stefan Rung, Cemal Esen, a Ralf Hellmann. 2021. „Compact Beam Homogenizer Module with Laser-Fabricated Lens-Arrays". *Applied Sciences* 11 (3): 1018. <https://doi.org/10.3390/app11031018>.
- Yang, Tongzhen, Minjing Li, Qing Yang, Yu Lu, Yang Cheng, Chengjun Zhang, Bing Du, Xun Hou, a Feng Chen. 2022. „Femtosecond Laser Fabrication of Submillimeter Microlens Arrays with Tunable Numerical Apertures". *Micromachines* 13 (8): 1297. <https://doi.org/10.3390/mi13081297>.